NASA/TM-20230015441

Tensile Behavior and High-Cycle Fatigue Durability of a SiC/SiC Ceramic-Matrix Composite Without and With Simulated Cooling Holes

Sreeramesh Kalluri
HX5, LLC, Brook Park, Ohio

Craig E. Smith, James D. Kiser, and Amjad S. Almansour
Glenn Research Center, Cleveland, Ohio

February 2024

NASA STI Program Report Series

Since its founding, NASA has been dedicated to the advancement of aeronautics and space science. The NASA scientific and technical information (STI) program plays a key part in helping NASA maintain this important role.

The NASA STI program operates under the auspices of the Agency Chief Information Officer. It collects, organizes, provides for archiving, and disseminates NASA's STI. The NASA STI program provides access to the NTRS Registered and its public interface, the NASA Technical Reports Server, thus providing one of the largest collections of aeronautical and space science STI in the world. Results are published in both non-NASA channels and by NASA in the NASA STI Report Series, which includes the following report types:

- TECHNICAL PUBLICATION.
  Reports of completed research or a major significant phase of research that present the results of NASA Programs and include extensive data or theoretical analysis. Includes compilations of significant scientific and technical data and information deemed to be of continuing reference value. NASA counterpart of peer-reviewed formal professional papers but has less stringent limitations on manuscript length and extent of graphic presentations.

- TECHNICAL MEMORANDUM.
  Scientific and technical findings that are preliminary or of specialized interest, e.g., quick release reports, working papers, and bibliographies that contain minimal annotation. Does not contain extensive analysis.

- CONTRACTOR REPORT.
  Scientific and technical findings by NASA-sponsored contractors and grantees.

- CONTRACTOR REPORT.
  Scientific and technical findings by NASA-sponsored contractors and grantees.

- CONFERENCE PUBLICATION.
  Collected papers from scientific and technical conferences, symposia, seminars, or other meetings sponsored or co-sponsored by NASA.

- SPECIAL PUBLICATION.
  Scientific, technical, or historical information from NASA programs, projects, and missions, often concerned with subjects having substantial public interest.

- TECHNICAL TRANSLATION.
  English-language translations of foreign scientific and technical material pertinent to NASA's mission.

Specialized services also include organizing and publishing research results, distributing specialized research announcements and feeds, providing information desk and personal search support, and enabling data exchange services.

For more information about the NASA STI program, see the following:

- Access the NASA STI program home page at http://www.sti.nasa.gov

NASA/TM-20230015441

Tensile Behavior and High-Cycle Fatigue Durability of a SiC/SiC Ceramic-Matrix Composite Without and With Simulated Cooling Holes

Sreeramesh Kalluri
HX5, LLC, Brook Park, Ohio

Craig E. Smith, James D. Kiser, and Amjad S. Almansour
Glenn Research Center, Cleveland, Ohio

National Aeronautics and
Space Administration

Glenn Research Center
Cleveland, Ohio 44135

February 2024

Acknowledgments

This work was funded by the NASA Hybrid Thermally Efficient Core Project. CMC test specimens were supplied by GE Aviation under NASA Glenn Research Center Contract NNC15BA05B/80GRC020R0004. Technical discussions with Roger Seither and Dane Dale (GE Aviation, Evendale, Ohio) were immensely helpful during this investigation. Authors are grateful to the high-cycle fatigue testing support provided by Daniel Gorican, Ralph J. Pawlik, and Ronald E. Phillips (Retired) and the scanning electron microscopy support from Wayne D. Jennings (HX5, LLC, NASA Glenn Research Center). This work was performed with continuous encouragement and management support received from Jon C. Goldsby and Joseph E. Grady (Retired) (NASA Glenn Research Center).

This work was sponsored by the Advanced Air Vehicles Program at the NASA Glenn Research Center.

Level of Review: This material has been technically reviewed by technical management.

This report is available in electronic form at https://www.sti.nasa.gov/ and https://ntrs.nasa.gov/

NASA STI Program/Mail Stop 050
NASA Langley Research Center
Hampton, VA 23681-2199

Tensile Behavior and High-Cycle Fatigue Durability of a SiC/SiC Ceramic-Matrix Composite Without and With Simulated Cooling Holes

Sreeramesh Kalluri
HX5, LLC
Brook Park, Ohio 44142

Craig E. Smith, James D. Kiser, and Amjad S. Almansour
National Aeronautics and Space Administration
Glenn Research Center
Cleveland, Ohio 44135

Summary

High-cycle fatigue (HCF) behavior of a melt-infiltrated, prepreg SiC/SiC composite was investigated using specimens without and with simulated cooling holes at 816 and 1,316 °C. The ceramic-matrix composite (CMC) material used for this study was fabricated by GE Aviation and had a ply configuration of $[0/90/0]_3$. HCF tests were conducted with an R-ratio of 0.6 and a cyclic frequency of 30 Hz. Maximum tensile gross-section stresses used in the HCF tests ranged from 152 to 359 MPa. Runout in HCF was defined as 30 million cycles (278 h) at both temperatures. Monotonic tensile tests were conducted at room temperature (RT) on as-received CMC specimens and on HCF runout specimens without and with holes to determine residual tensile strengths. Digital image correlation (DIC) and acoustic emission (AE) techniques were used to monitor progression of damage in RT tensile tests on specimens without and with holes. Fractography was performed on a limited number of specimens without and with holes to determine morphology of fracture surfaces. Representative RT stress-strain behavior, elevated-temperature HCF behavior at the two temperatures, and RT residual tensile strengths of HCF runout specimens are documented in this report. Select examples of DIC and AE data from RT tensile tests on specimens without and with holes and typical features observed on fracture surfaces of specimens tested under tensile and HCF conditions are also discussed.

Introduction

Next-generation gas turbine engines are required to achieve greater thermodynamic efficiency and decrease specific fuel consumption by operating at higher temperatures and pressure ratios. Ceramic-matrix composites (CMCs) exhibit low density (approx. one-third that of superalloys) and retain their strength at elevated temperatures, which allows higher inlet temperatures for turbine engine components fabricated from CMCs compared to superalloys. Lewis et al. described application of uncooled CMCs for power turbine blades to improve performance of advanced turboshaft engines (Ref. 1). Since CMC turbine components can tolerate higher temperatures than similar superalloy components, the amount of cooling air required to cool CMC components tends to be less. Additionally, active cooling of CMC components is feasible with cooling holes fabricated in CMC components, if required by the design. Turbine blades are subjected to large centrifugal forces (generated by high rotational speeds of the turbine) and vibratory loads at high frequencies. The objectives of the current investigation are to evaluate high-temperature, high-cycle fatigue (HCF) behavior of a prepreg SiC/SiC CMC without and with

simulated cooling holes and to determine the room-temperature (RT) retained tensile strength of the CMC from specimens that did not fail at high temperatures after HCF testing.

Material and Test Specimens

SiC/SiC CMC was fabricated by GE Aviation using a prepreg-melt infiltration (MI) process. The SiC/SiC composite consisted of biased $[0°/90°/0°]_3$ architecture with each ply comprising unidirectional tape material fabricated using Hi-Nicalon^{TM} Type S fiber tows (NGS Advanced Fibers Co., Ltd.) via the wet drum winding process. The fibers are typically coated with a weak interphase. After the desired ply layup preforming, the subsequent steps included compaction and densification with silicon MI. The entire fabrication process of the CMC is described in detail by Steibel (Ref. 2). Machined dog-bone-type tensile specimens with the following dimensions were supplied by GE Aviation: 152 mm overall length with nominal gage section width and thickness of 10.2 and 2.0 mm, respectively. Uniform gage length in these specimens without holes was 25.4 mm. Similar geometry tensile specimens were successfully used to investigate high-temperature tensile and fatigue behaviors of CMCs (Refs. 3 and 4). In a second set of tensile specimens, five evenly spaced 0.66-mm-diameter holes were drilled within the gage section at an angle of 20° to the surface of the specimen, perpendicular to the loading direction, using electric discharge machining. These holes were designed to simulate cooling airholes, which are needed in a cooled CMC turbine blade. In a plane perpendicular to the loading direction, the load-bearing cross-sectional area of the tensile specimen was reduced by 23 percent because of the presence of simulated cooling holes. The net-section load-bearing cross-sectional area was determined by measuring the average hole size with an optical profilometer and calculating the reduced cross-sectional area. The machined specimen edges and holes were not seal coated.

Experimental Details

Tensile test rigs were aligned with a strain-gage alignment specimen to ensure bending strains were less than 5 percent of the axial strain at an applied tensile force of 4.4 kN. HCF test specimens were heated in a dual-zone, commercially available igniter furnace (AMTECO). Three equally spaced, type-R thermocouples were bonded within the gage section of the test specimen to determine temperature distribution. With the dual-zone igniter furnace, temperatures within the gage section of the test specimens were within $\pm$1 percent of the required test temperatures (816 and 1,316 °C). High-temperature, HCF tests were conducted at 816 and 1,316 °C in force control with an R-ratio (min. stress/max. stress in a cycle) of 0.6 at a frequency of 30 Hz on specimens without and with holes. Those temperatures are considered to be (1) an intermediate temperature where pesting from oxidation has traditionally been a concern (816 °C) (Ref. 5) and (2) a maximum, long-term operating temperature for MI SiC/SiC (1,316 °C). Runout in a HCF test was defined as 30 million cycles (278 h).

Baseline and residual tensile properties were determined from as-fabricated (pristine) and HCF runout specimens, respectively. Specimens without and with holes were tested in displacement control (displacement rate: 0.01 mm/s) at RT. For tensile specimens with holes, gross-section cross-sectional areas (not considering the holes) were used to determine stresses (and force values) to control the HCF tests. Subsequently, these gross-section stress values were used to determine the net-section stresses by accounting for the reduction in cross-sectional areas due to holes. As mentioned earlier, net-section stresses were determined by measuring the average hole sizes with an optical profilometer and calculating the reduced cross-sectional area. In all the HCF tests on specimens with holes, failures typically occurred at one of the outermost cooling holes. Digital image correlation (DIC) and acoustic emission (AE) techniques were used to monitor damage progression in the specimens. DIC images were obtained with

two pairs of 8.9-megapixel forward-looking infrared (FLIR) cameras and analyzed with DIC software (from Correlated Solutions, Inc.). Modal AE was monitored with four sensors, each with a frequency range of 50 kHZ to 2.0 MHz, located outside the gage. Sensors were clamped to the samples with vacuum grease couplant, and waveforms were recorded with hardware and software from Digital Wave Corporation (currently, Hexagon Digital Wave). Vertical location of the acoustic events was determined by the arrival time difference on inner sensors (closest to the gage section). The changing speed of sound upon cracking was accounted for by the outer sensors (farthest from the gage section). Only events that originated within the gage were included in the analysis. In addition, a capacitance contact extensometer with $\pm$1 percent range was also used to monitor strains in the 25.4-mm gage sections of tensile specimens.

Experimental Results and Discussion

RT Baseline Tensile Tests

Because of limited availability of test specimens, only two tensile tests (one monotonic and a second one of load-unload type to capture hysteresis) were conducted on as-fabricated (pristine) specimens without and with holes at RT. Strains were calculated from displacements measured with a 25.4-mm-gauge-length extensometer. Monotonic tensile stress-strain curves obtained from these tests are shown in Figure 1(a) and 1(b) for gross-section stress versus strain and net-section stress versus strain, respectively. As expected, on a gross-section stress basis, the tensile curve for the specimen with holes is lower than that obtained for the specimen without holes. However, on a net-section stress basis, both tensile curves are similar at least up to the transition knee, which separates the linear region from the nonlinear region. Proportional limit strength (PLS, 0.005 percent offset) and in-plane tensile strength (ITS) values of baseline CMC specimens without and with simulated cooling holes are shown in Table I. When compared on a net-section stress basis, PLS and ITS values of the specimens without and with holes are somewhat similar. The failure strain of the specimen with holes was significantly less than that of the specimen without holes (Figure 1(a) and 1(b)). To capture variability in the tensile data, it is desirable to conduct multiple tests on each type of test specimens both at room as well as at high temperatures where the HCF test data are generated.

HCF Fatigue Behavior at 816 and 1,316 °C

HCF data generated on the CMC at 816 and 1,316 °C are shown in Figure 2 and Figure 3, respectively. For 816 °C, fatigue data are plotted on a maximum gross-section tensile stress versus cyclic life basis in Figure 2(a), and the same data are plotted on a maximum tensile net-section stress versus cyclic life basis in Figure 2(b). For 1,316 °C, similar plots are shown in Figure 3(a) and (b). Runouts (specimens that completed 30 million cycles and did not fail during HCF testing) are identified in these images. HCF data from specimens without and with holes are presented, as are the observed trends for each fatigue data set. At both temperatures, as expected on a gross-section maximum stress basis, specimens with simulated cooling holes exhibit lower fatigue lives than those observed for specimens without holes. On a net-section maximum stress basis, at 816 °C the difference in HCF fatigue lives between the specimens without and with simulated cooling holes is reduced (Figure 2(b)). However, at 1,316 °C the difference in HCF fatigue lives between the specimens without and with simulated cooling holes is evident (Figure 3(b)), which is indicative of a fatigue stress concentration factor (K_f) that is greater than unity at this temperature. This might be partly due to accumulated cyclic creep damage, but oxidation damage in cracks emanating from a machined hole was also observed via fractography in specimens that failed during 1,316 °C HCF testing. As mentioned earlier, due to limited availability of

test specimens, only one HCF test was conducted per maximum gross-section stress and high-temperature test condition on specimens without and with holes. To account for scatter that is common in CMC fatigue data (Ref. 6), HCF tests should be conducted on multiple specimens without and with holes for each test condition to confirm trends observed at both temperatures in this study.

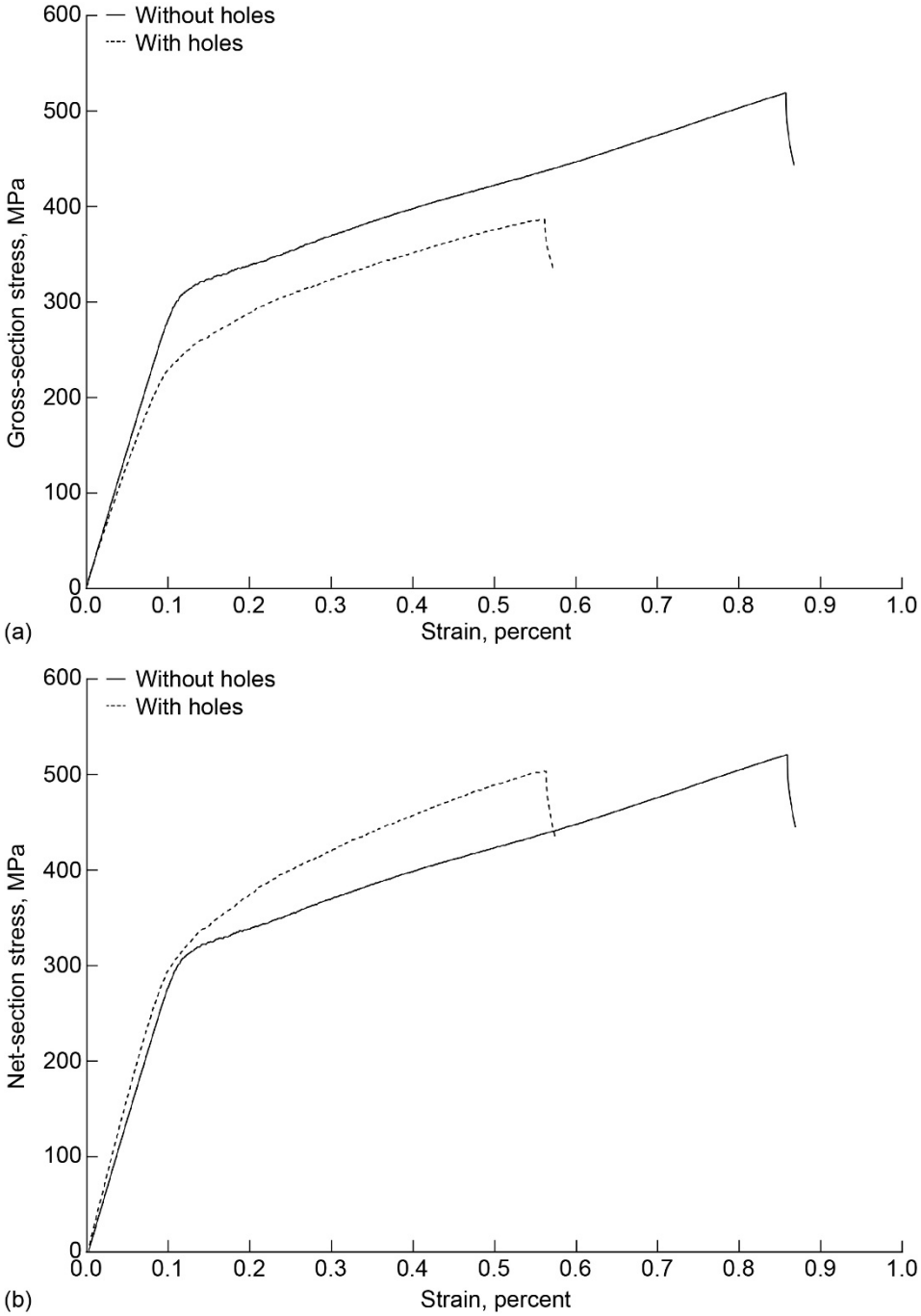

Figure 1.—Baseline tensile stress-strain curves at RT for pristine SiC/SiC CMC.
(a) Gross-section stress and strain. (b) Net-section stress and strain.

TABLE I.—RT TENSILE PROPERTIES OF
BASELINE (PRISTINE) SiC/SiC CMC SPECIMENS

Test type	Specimens without holes[a]		Specimens with holes[b]	
	0.005% offset PLS, MPa	ITS, MPa	0.005% offset PLS, MPa	ITS, MPa
Monotonic	290	520	260	488
Load/unload (hysteresis)	300	504	314	496

[a]Gross-section stress values.
[b]Net-section stress values.

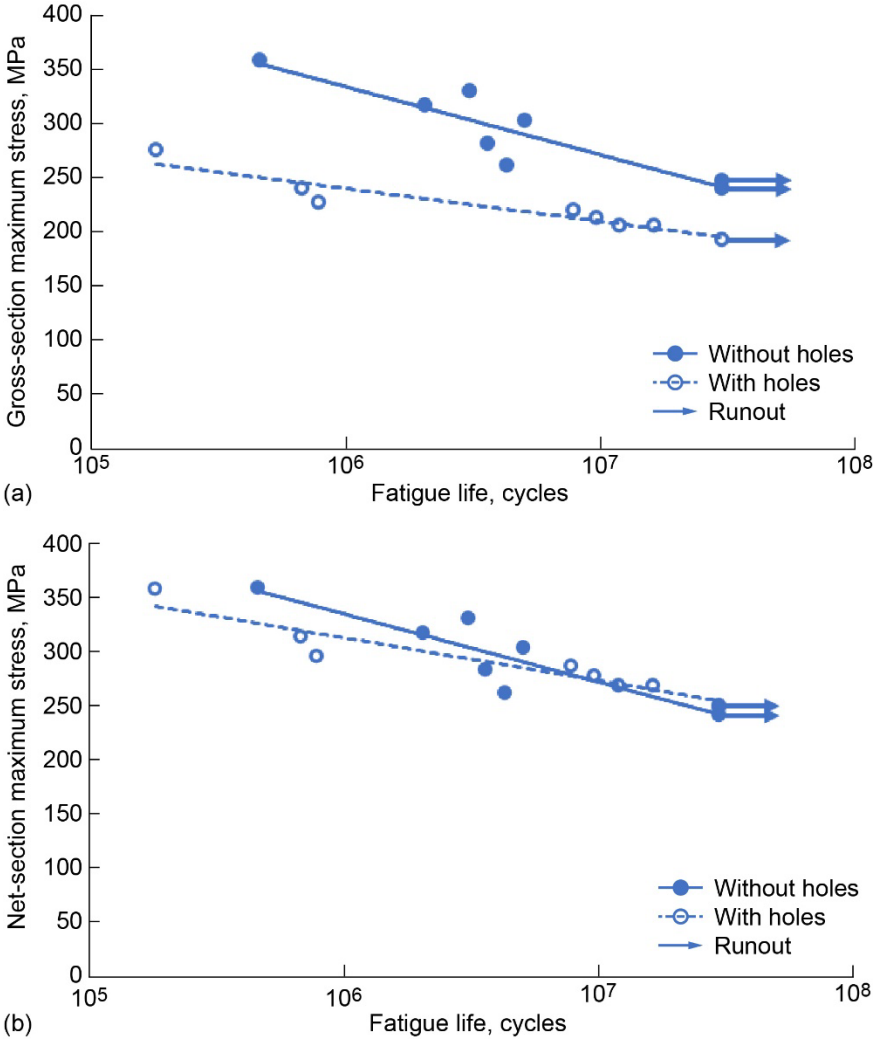

Figure 2.—HCF data for SiC/SiC CMC at 816 °C. (a) Gross-section maximum stress versus fatigue life. (b) Net-section maximum stress versus fatigue life.

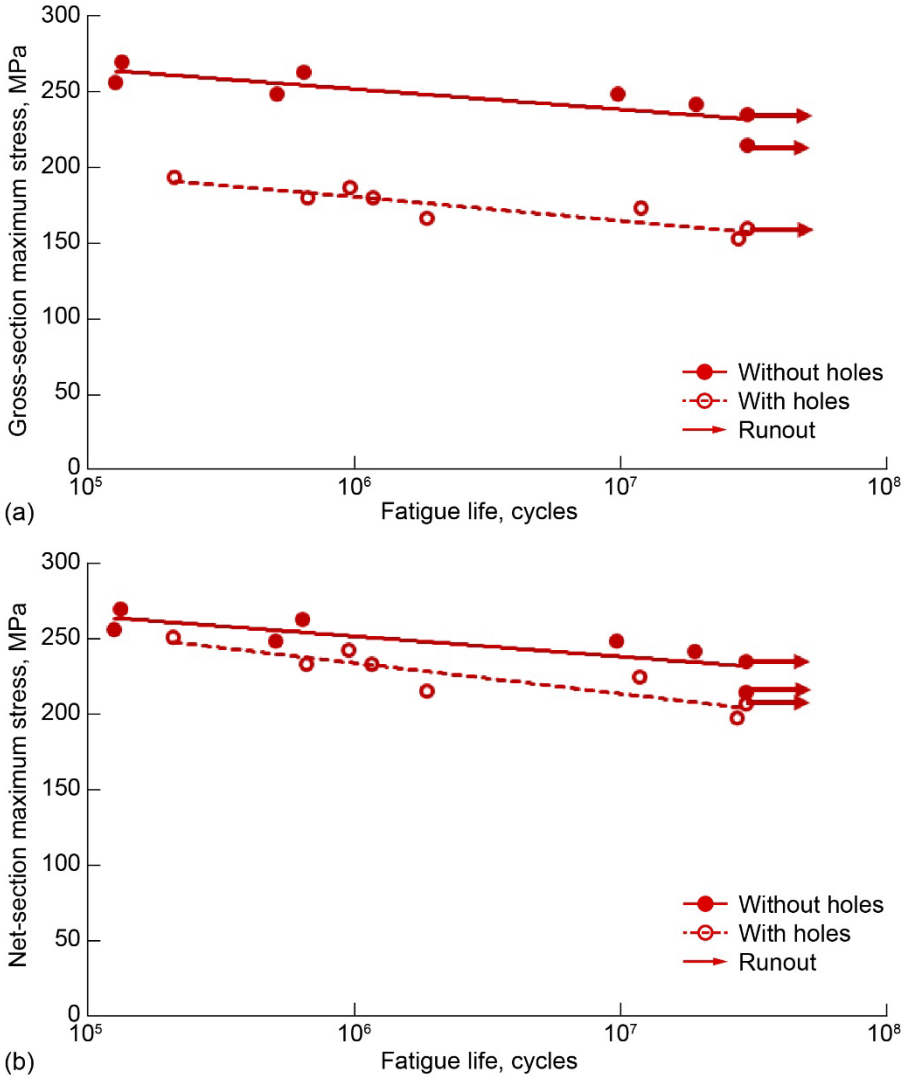

Figure 3.—HCF data for SiC/SiC CMC at 1,316 °C. (a) Gross-section maximum stress versus fatigue life. (b) Net-section maximum stress versus fatigue life.

RT Tensile Tests on HCF Runout CMC Specimens

The RT tensile tests were conducted in displacement control to determine retained tensile strength of HCF runout specimens without and with simulated cooling holes. Stress-strain curves from these tests are shown using both gross- and net-section stresses in Figure 4. For comparison, similar stress-strain curves obtained on pristine CMC specimens without and with holes are also included in Figure 4. As in the case of pristine specimens, on a gross-section stress basis, PLS values of specimens with simulated cooling holes (tested for retained strength) are lower compared to corresponding PLS values for specimens without holes. The retained PLS value of the runout specimen without holes tested in HCF at 1,316 °C is much lower compared to PLS values of those tested at 816 °C (Figure 4(a)). On a net-section-stress basis, PLS values of retained strength from specimens with simulated cooling holes are similar to that observed for the baseline specimen. However, the retained PLS value of the runout specimen without holes tested at 1,316 °C is still much lower than the PLS values of the retained-strength runout specimens tested in HCF at 816 °C (Figure 4(b)). Lower retained in-plane tensile strength values observed for runout specimens tested in HCF at both temperatures, without and with holes, indicate damage due to prior HCF cycling. In particular, the runout samples with holes showed greatly reduced strain to failure and ITS, indicating a reduction in material capability.

Acoustic Emission (AE) and Digital Image Correlation (DIC) Results From Baseline and Retained-Strength Tensile Tests on HCF Runout CMC Specimens

Normalized AE energy from RT tensile tests on baseline and HCF runout specimens without and with holes is plotted against gross- and net-section stresses in Figure 5. In this figure, the cumulative AE energy released for each test is normalized to the total value so that AE energies from different test specimens can be readily compared. Onset of acoustic events appears to occur at lower gross-section stresses in specimens with simulated cooling holes when compared with similar stresses for specimens without holes (Figure 5(a)). However, differences in the stress levels triggering onset of acoustic events diminish between specimens without and with simulated cooling holes when viewed on a net-section stress basis (Figure 5(b)).

Table II lists cracking stress values (on a net-section basis) obtained from the as-fabricated (pristine) specimens and retained-strength HFC runout tests at RT. The PLS values were determined by a 0.005-percent strain offset method. The first AE event and the first loud AE event detected in the gage section are indications of the first occurrence of microcracking (typically in transverse plies) and the first occurrence of matrix cracking, respectively (Ref. 7). First loud AE event is defined as the first event that has energy within an order of magnitude of the loudest event detected throughout the test. AE onset stress is determined by a linear regression of the linear segment of the curves in Figure 5(b), and it gives an indication of when cracks link up through the thickness (Ref. 7). The stress when local strain accumulation was first observed in DIC images is also listed in Table II.

On a net-section basis, the first AE event was between 172 and 194 MPa for as-fabricated (pristine) specimens without holes and between 56 and 58 MPa for specimens with holes. The presence of holes led to microcracking at lower stresses. The first loud AE event occurred between 232 and 245 MPa for specimens without holes and between 141 and 185 MPa for specimens with holes. This indicates that matrix cracking occurs at a lower stress for the samples with holes, which is supported by the first DIC stresses (Figure 6). AE onset stresses for all samples are within 34 MPa of each other, with the specimen 14947-TD4 (HCF tested at 234 MPa without holes) being slightly lower than others.

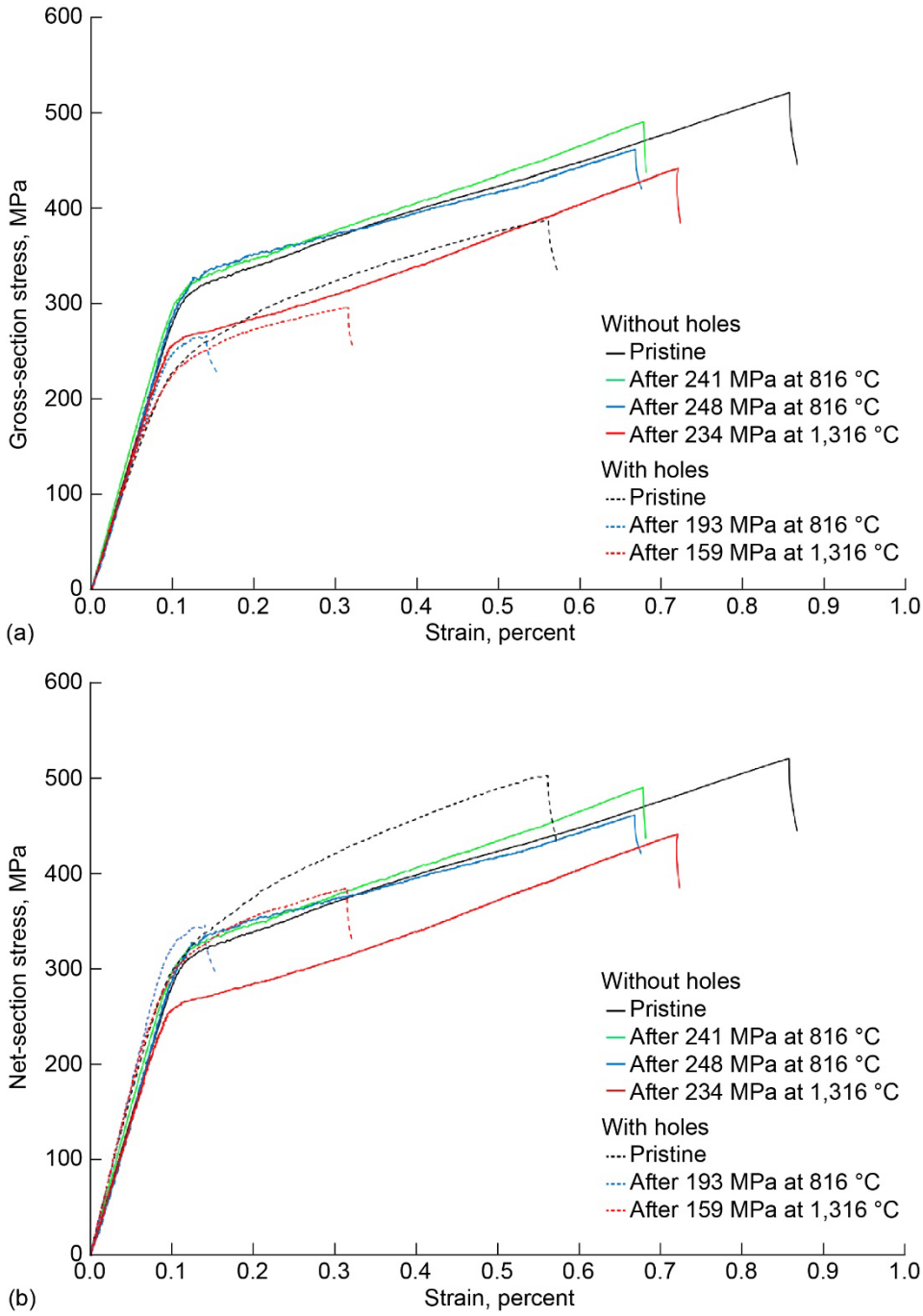

Figure 4.—RT tensile stress-strain curves from retained-strength tests for SiC/SiC CMC. (a) Gross-section stress and strain. (b) Net-section stress and strain.

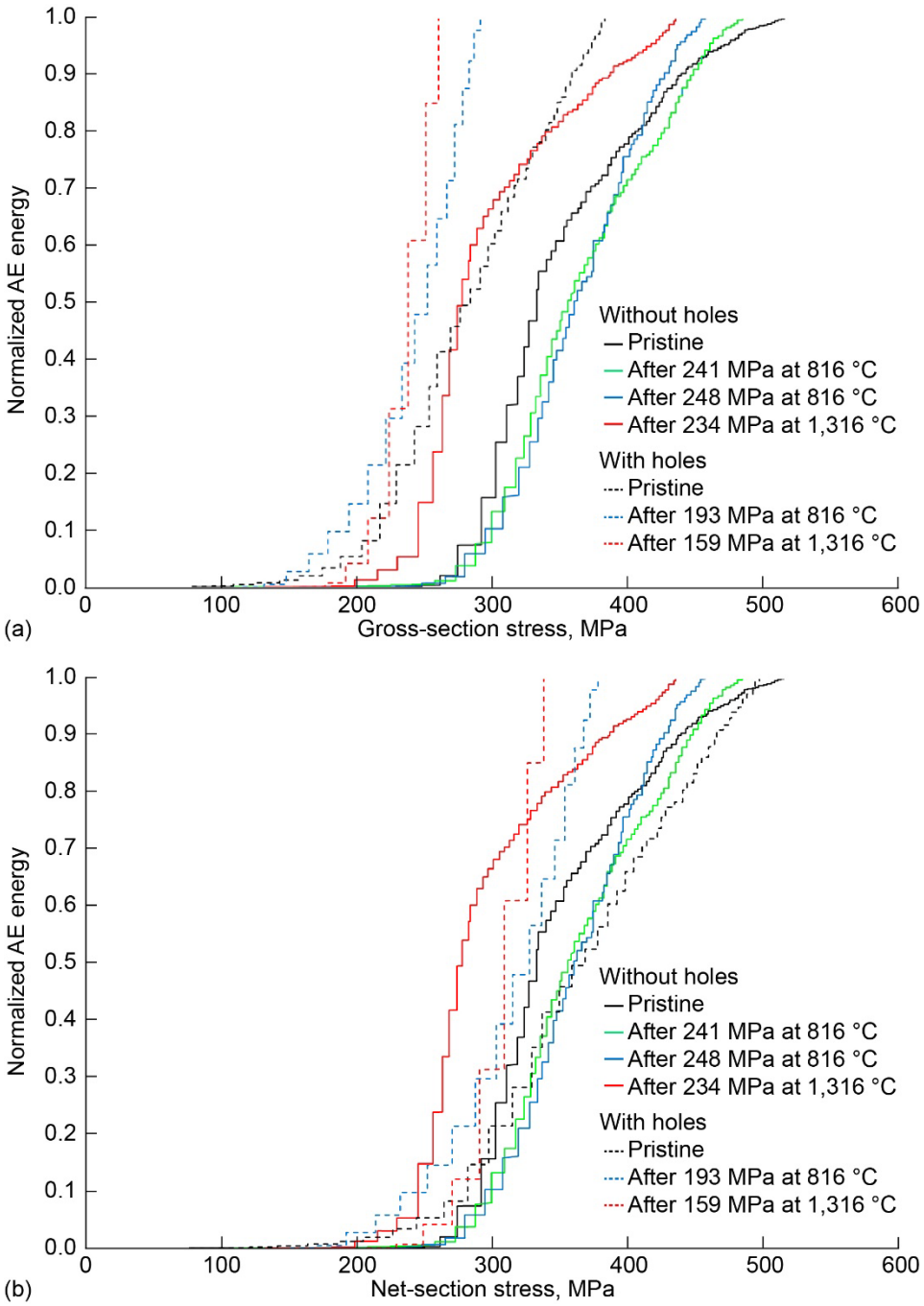

Figure 5.—Normalized AE energies from RT tensile tests on HCF runout SiC/SiC CMC specimens. Normalized AE energies from baseline RT tensile tests on pristine CMC specimens are included for comparison. (a) Gross-section stress. (b) Net-section stress.

TABLE II.—CRACKING STRESS VALUES (ON NET-SECTION BASIS) OBTAINED FROM TENSILE TESTS ON AS-FABRICATED (PRISTINE) AND RETAINED-STRENGTH TESTS ON RUNOUT HCF SiC/SiC CMC SPECIMENS AT RT

Specimen number	Test conditions	0.005% offset PLS, MPa	First AE, MPa	First loud AE, MPa	AE onset, MPa	Initial DIC, MPa
Without holes						
14950-TD5	Pristine	290	194	245	276	288
14951-TD5	Pristine, load-unload or hysteresis	300	172	232	269	281
14947-TD3	Retained strength, after 241 MPa HCF at 816 °C	300	107	257	283	273
14951-TD4	Retained strength, after 248 MPa HCF at 816 °C	320	168	233	293	247
14947-TD4	Retained strength, after 234 MPa HCF at 1,316 °C	255	132	199	234	248
With holes[a]						
14948-TD2	Pristine	260	56	185	260	218
14949-TD1	Pristine, load-unload or hysteresis	314	58	141	268	219
14953-TD1	Retained strength, after 193 MPa HCF at 816 °C	318	208	249	278	136
14953-TD2	Retained strength, after 159 MPa HCF at 1,316 °C	247	150	170	269	203

[a]For specimens with holes, test conditions listed are gross-section stress values and not net-section stress values.

For specimen 14953-TD1, the low stress for the initial DIC and the high stress for the first AE and first loud AE indicates preexisting damage from HCF. Cracks that formed during HCF were not detected by AE but they would be expected to open up upon loading at RT and appear on DIC without generating new AE. Specimens 14953-TD1 and 14951-TD4 were loaded in HCF at the same net-section stress conditions. The first loud AE, AE onset, and PLS were similar. The first AE was lower for the specimen without holes, while the initial DIC was lower for the specimen with holes. This may be explained by preexisting cracks in specimen 14953-TD1 due to previous HCF cycling.

Full-field images of strain in the loading direction were obtained from post-processed deformation images acquired by a 3D DIC system on both sides (A and B) of baseline and HCF runout specimens without and with holes during tensile testing (Figure 6 and Figure 7). Gross-section stress levels corresponding to each pair of images are included in these figures. Increase in the density of strain bands with an increase in the gross-section stress and final failure occurring from one of the higher magnitude strain bands in the baseline test specimen without holes can be seen in Figure 6(a). The two notch-like features in this figure are shadows from the extensometer probes. Similar full-field strain plot for a baseline specimen with holes tested under tensile loading is shown in Figure 6(b). In the specimen with holes, strain bands originate from the ends of holes at lower gross-section stresses, which become more pronounced as the gross-section stress increases leading to final failure from the top hole. Full-field strain images in the loading direction for HCF runout specimens tested at 248 MPa and 816 °C and also at 234 MPa and 1,316 °C are shown in Figure 7. In both HCF runout specimens tested at 816 and 1,316 °C, first indication of strain band in DIC appeared at a similar gross-section stress (Figure 7(a) and (b)). The 1,316 °C specimen showed through-thickness cracks earlier, as verified by AE onset and PLS. This might be due to localized damage in the CMC due to prior HCF testing at 1,316 °C.

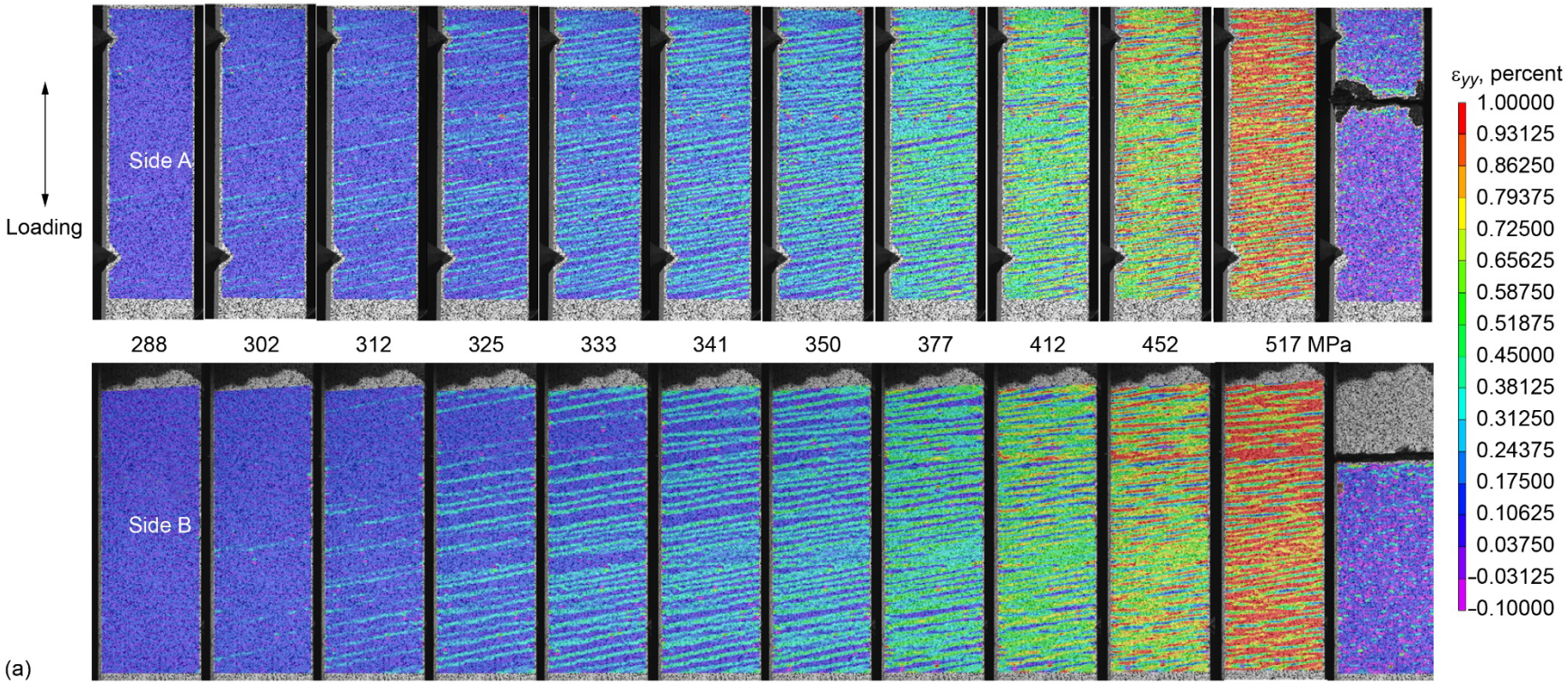

Figure 6.—DIC images of strain in loading direction (ε_{yy}) from RT tensile tests on SiC/SiC CMC baseline specimens. Gross-section stresses corresponding to each pair of images (side A and side B) are shown. (a) Without holes. (b) With holes.

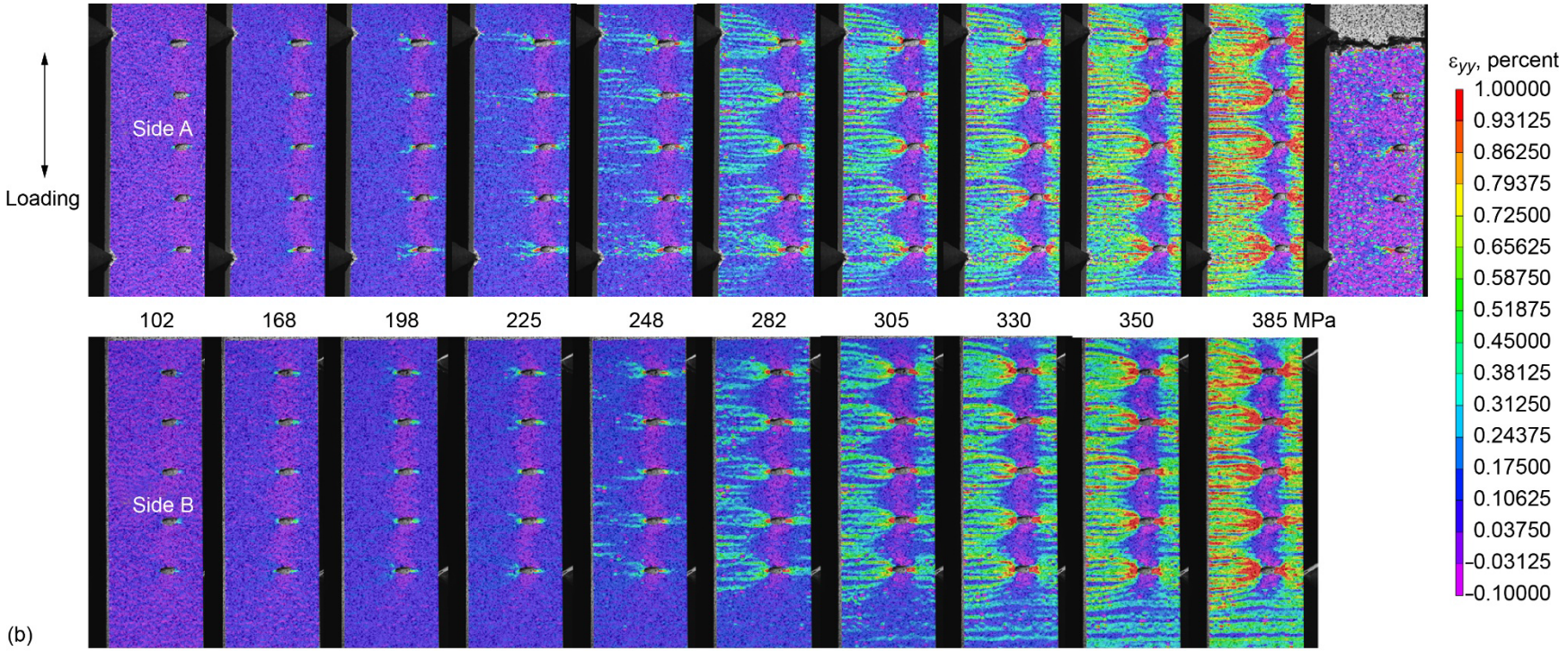

(b)

Figure 6.—Concluded.

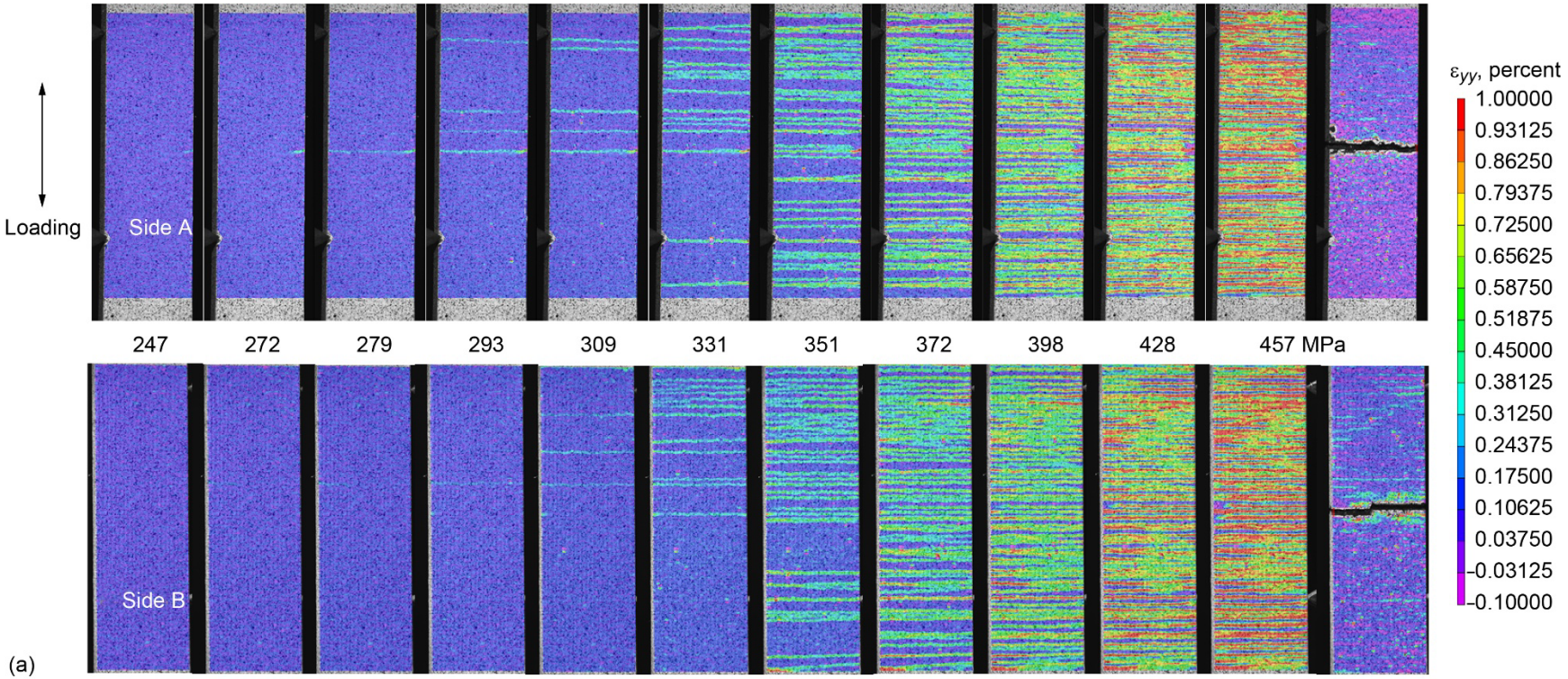

Figure 7.—DIC images of strain in loading direction from RT tensile tests on CMC HCF runout specimens without holes. Gross-section stresses corresponding to each pair of images (side A and side B) are shown. (a) Tested at 248 MPa and 816 °C. (b) Tested at 234 MPa and 1,316 °C.

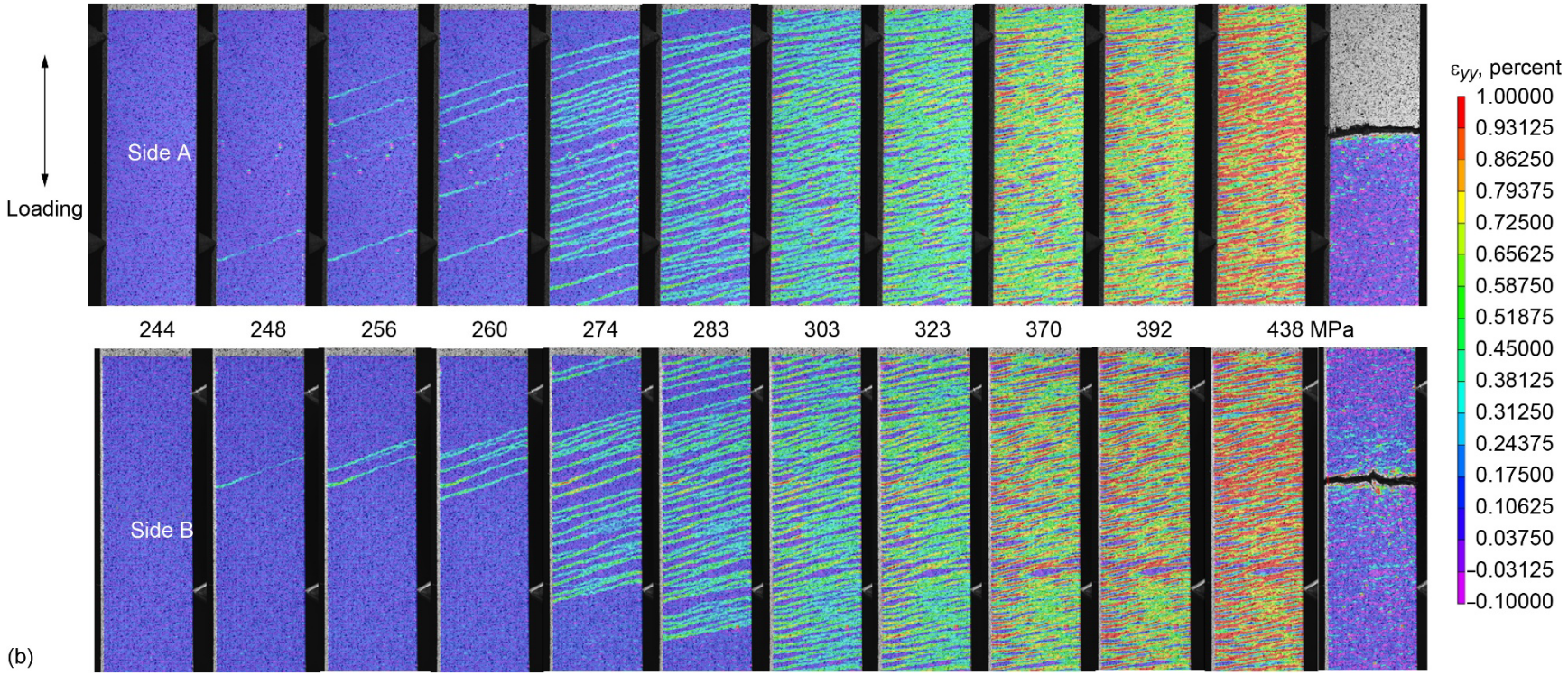

(b)

Figure 7.—Concluded.

Fractography of Baseline Tensile Test Specimens

Fracture surface images of a baseline specimen tested at RT under tension to failure are shown in Figure 8. Significant fiber pullout was observed throughout the fracture surface along with holes that were left behind after the fibers pulled out (indicated with red arrows).

Fractography of HCF Test Specimens at 816 and 1,316 °C

Fractography was performed on a limited number of failed HCF specimens without and with holes tested at 816 and 1,316 °C. Examples of fracture surfaces from two specimens without holes tested in HCF at 816 °C are shown in Figure 9. Unlike the specimens subjected to tensile loading alone, the specimens tested in HCF at 816 °C exhibited some areas with limited or no fiber pullout within 0° plies, indicating the presence of oxidation (identified by yellow arrows). No glassy phase was present on the fracture surfaces of HCF specimens tested at 816 °C. Morscher (Ref. 5) had noted that at the

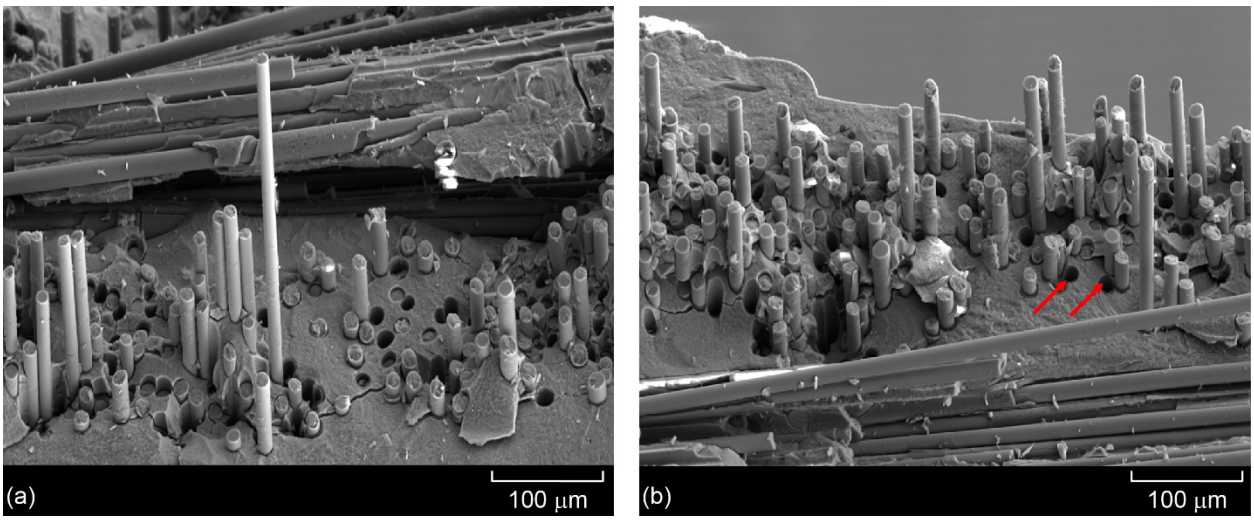

Figure 8.—Fracture surface of baseline CMC specimen without holes tested in tension at RT.

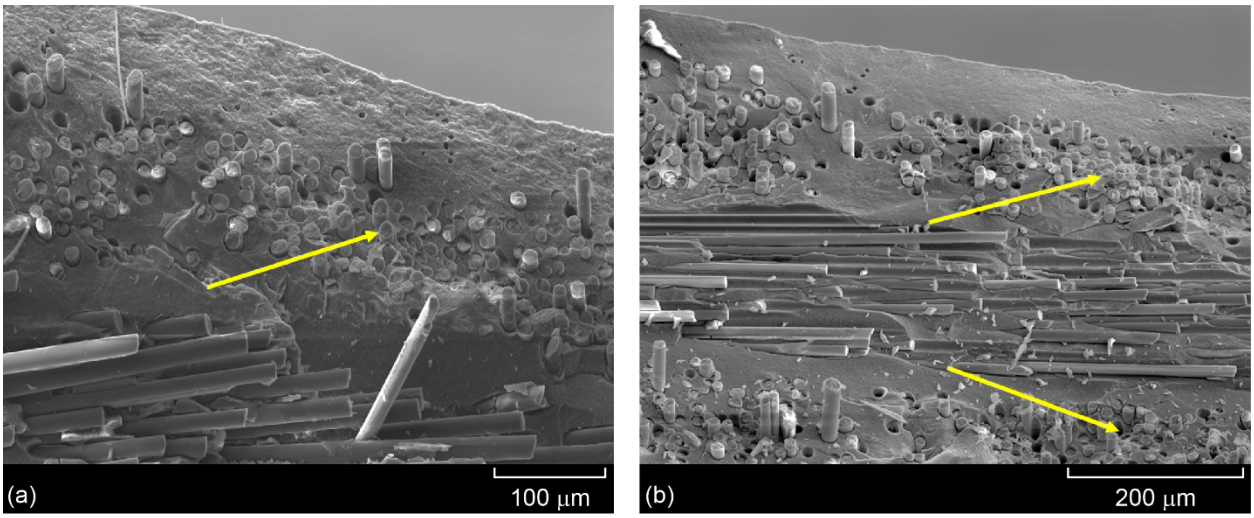

Figure 9.—Fracture surfaces of CMC specimens without holes tested in HCF at 816 °C. (a) Gross-section maximum stress, 317 MPa; 19 h to failure. (b) Gross-section maximum stress, 359 MPa; 4.3 h to failure.

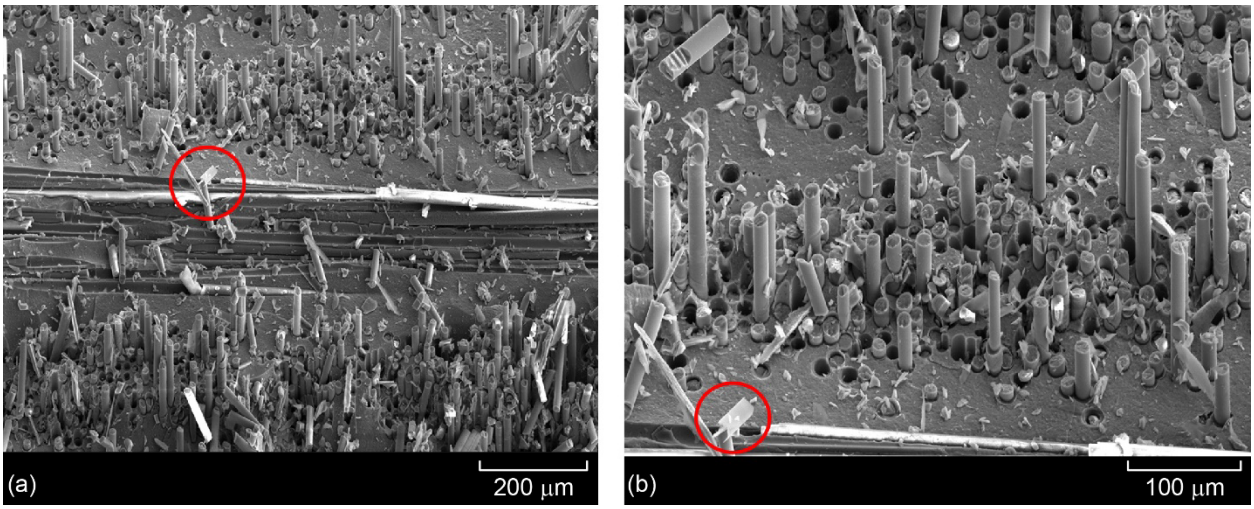

Figure 10.—Fracture surface of CMC specimen without holes tested in HCF at 1,316 °C and gross-section maximum stress of 241 MPa; 179 h to failure.

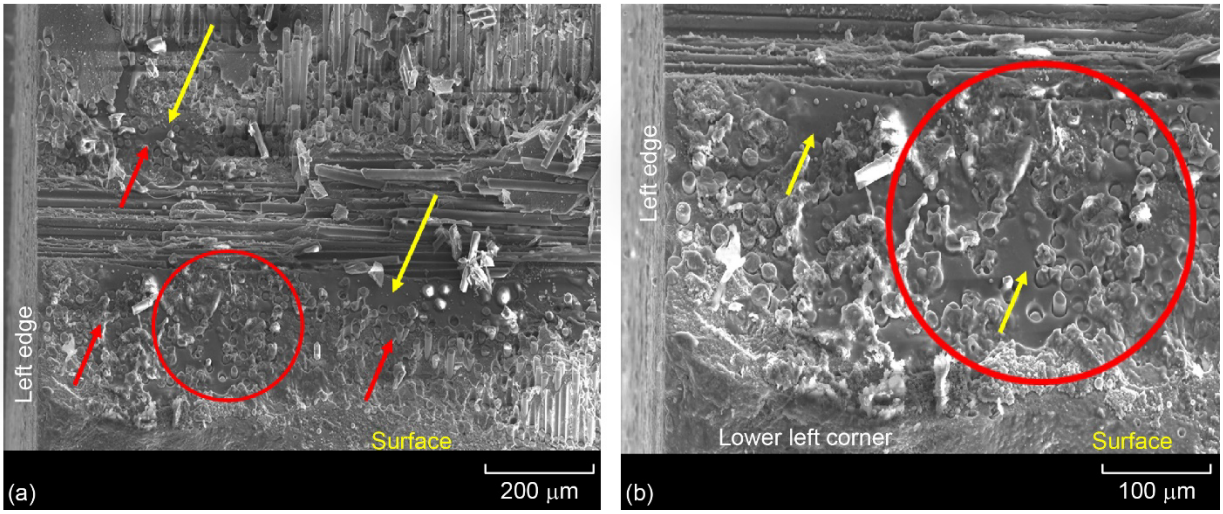

Figure 11.—Fracture surface of a CMC specimen without holes tested in HCF at 1,316 °C and gross-section maximum stress of 248 MPa; 4.7 h to failure.

“intermediate temperature,” fiber-matrix bonding can result in local stress concentration on the fibers in the region of a matrix crack (from oxidation). The sample that failed in only 4.3 h was subjected to a stress that was much higher than the RT PLS of approximately 280 MPa. Examples of fracture surfaces from two specimens without holes tested in HCF at 1,316 °C are shown in Figure 10 and Figure 11. Significant fiber pullout was observed throughout the specimen tested at 1,316 °C and 241 MPa gross-section maximum stress for 179 h (Figure 10). This sample was tested at a stress slightly above the apparent runout stress. In contrast, oxidized and embrittled areas were evident in the specimen tested at 1,316 °C and 248 MPa gross-section maximum stress for 4.7 h (Figure 11). Embrittled regions where the 0° fibers failed (red circle and arrows) and smooth regions that appear glassy with oxidation (yellow arrows) were observed; however, there were other undamaged areas with extensive fiber pullout. Thus, at 1,316 °C significant amounts of glassy phase can form within an open crack in <5 h, and fibers in those areas are embrittled. It is surprising to see the variation in specimen life with small changes in stress at 1,316 °C, but the fractography shows the type of significant damage that can occur in open cracks.

Linear Crack Density Results on Tested Tensile and HCF Specimens

Sections from the gage of specimens without holes were cut, mounted, and polished parallel to the edge, and sections from the gage of specimens with holes were cut, mounted, and polished parallel to the face. For specimens without holes, the polished sections were taken from one as-fabricated (pristine) specimen that was tested in monotonic or fast fracture (FF) tension, one specimen that achieved HCF runout at 816 °C and was then tested in FF tension, and one specimen that achieved HCF runout at 1,316 °C and was then tested in FF tension. The FF tensile tests were performed at RT. Microstructural characterization was performed on specimens polished parallel to the "face" of three specimens with holes under the same testing conditions of the specimens that were polished parallel to the edge, but cracks were hard to find in the face-polished specimens.

Figure 12(a) and (b) show low- and high-magnification images, respectively, of a polished edge from an as-fabricated (pristine) specimen that was tested in FF tension at RT. RT cracks were marked (in red) and counted in all 0° plies, averaged, and divided by the appropriate length to calculate the linear crack density, which is 3.4 cracks/mm. The initiation and propagation of the RT cracks during the FF tensile test of the as-fabricated (pristine) specimen was a result of increasing applied stress beyond the PLS through crack saturation and failure. Figure 12(c) and (d) show low- and high-magnification images, respectively, of a polished edge from a specimen that achieved runout at 816 °C then was FF tested in tension at RT. Cracks that formed during HCF testing at 816 °C are noted (in yellow) in Figure 12(d). Likewise, the cracks that were formed during tensile testing at RT are noted (in red) in Figure 12(b) and (d). Cracks that formed during HCF testing at 816 °C were mainly concentrated in the two inner 0° plies. Therefore, cracks were counted in the two inner 0° plies, averaged, and divided by the appropriate length to calculate the crack density, which is 5.2 cracks/mm. The formation of the cracks during the HCF testing at 816 °C was a result of cyclic mechanical loading without the presence of relaxation or creep at 816 °C, which prevented the matrix from accommodating the accumulation of cyclic-loading-induced strains without cracking. Figure 12(d) shows several cracks that formed during HCF testing at 816 °C, with one of them extending during the post-runout RT FF tensile test. Moreover, cracks that formed during HCF testing at 816 °C show oxidation damage likely due to the formation and spalling of borosilicate melt in the vicinity of the cracks. For CMCs that have a boron-nitride- (BN-) containing interphase, it was previously shown that in the vicinity of matrix cracks, the SiC fibers and matrix react with oxygen and form silica (SiO_2), and the BN in the interphase reacts with oxygen to form boria (B_2O_3) melt (Ref. 8), where the fluxing of the B_2O_3 melt with SiO_2 can further enhance SiC oxidation. Figure 12(e) and (f) show low and high magnification images, respectively, of polished edge samples from a specimen that achieved runout at 1,316 °C, then was tested in FF tension at RT. Cracks that formed during HCF testing at 1,316 °C are noted (in yellow) in Figure 12(f), and cracks that were formed during FF tensile testing at RT are noted (in red) in Figure 12(e) and (f). The number of cracks observed in this specimen was much lower than that of the two polished samples described previously, and as a result, crack density was not calculated. The lack of high-temperature crack formation in this specimen is likely due to relaxation and creep that occurs in SiC-based CMCs when mechanically loaded at temperatures above 1,200 °C. The relaxation and creep allowed the matrix to accommodate the accumulation of cyclic-loading-induced strains without cracking. Figure 12(f) shows a crack that formed during HCF testing at 1,316 °C filled with solid borosilicate glass oxide and extending during the post runout RT FF tensile test.

The reaction of SiO_2 and B_2O_3 forms a borosilicate glass melt that at high temperatures (>1,100 °C) eventually solidifies into a glass with high SiO_2 content (Ref. 8) that can seal the crack as shown in Figure 12(f) in HCF testing at 1,316 °C. However, the solid borosilicate glass can strongly bond (embrittle) the fibers, fusing adjacent fibers together, and embrittling CMCs (Ref. 8).

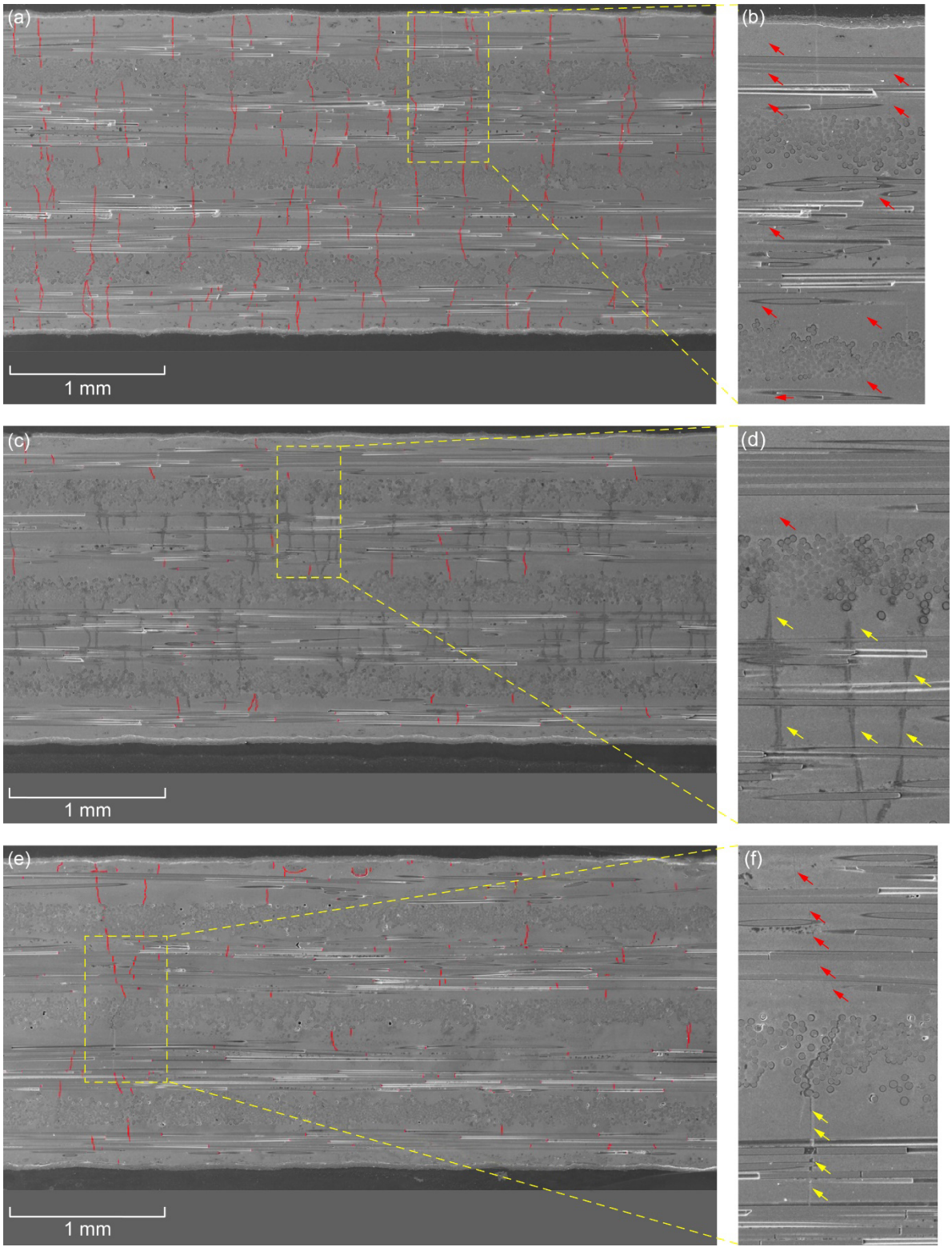

Figure 12.—Images of polished edges from SiC/SiC CMC specimens tested in FF tension at RT. (a) Low magnification, as-fabricated. (b) High magnification, as-fabricated. (c) Low magnification, prior HCF runout at 816 °C. (d) High magnification, prior HCF runout at 816 °C. (e) Low magnification, prior HCF runout at 1,316 °C. (f) High magnification, prior HCF runout at 1,316 °C.

Summary of Results

Experimental characterization of a melt-infiltrated, prepreg SiC/SiC ceramic-matrix composite (CMC) performed in this investigation, the results obtained, and conclusions are as follows:

1. Room-temperature (RT) baseline tensile strength tests were conducted on CMC specimens without and with simulated cooling holes. When compared on a net-section stress basis, proportional limit strength (PLS) and in-plane tensile strength (ITS) values of baseline CMC specimens without and with simulated cooling holes were somewhat similar.

2. High-temperature, high-cycle fatigue (HCF) behavior of CMC specimens without and with simulated cooling holes was characterized by conducting fatigue tests at 816 and 1,316 °C. When compared on a net-section stress basis, HCF lives of the CMC specimens with holes were somewhat lower compared to those from CMC specimens without holes; more so at 1,316 °C than at 816 °C. This might be due to cyclic creep and oxidation within cracks formed during HCF at the higher temperature.

3. Retained tensile strengths of HCF runout CMC specimens without and with simulated cooling holes tested at 816 and 1,316 °C were determined at RT. On a net-section stress basis, PLS values of specimens with simulated cooling holes (baseline and retained strength) were similar with one exception (PLS value of the runout specimen without holes tested in HCF at 1,316 °C). Lower retained ITS values observed for runout specimens without and with holes indicated damage due to prior HCF loading.

4. HCF tests and tensile strength tests should be conducted on multiple specimens without and with holes to confirm trends observed at both temperatures in this study. In addition, tensile strength tests at high temperatures would also be useful to understand the CMC behavior at those temperatures. In testing with one sample per HCF condition, the net-section maximum stress at runout of 30 million cycles was approximately 250 MPa at 816 °C (both without and with holes), and approximately 230 and 200 MPa at 1,316 °C for samples without and with holes, respectively.

5. HCF CMC specimens tested at 816 °C exhibited embrittled regions where oxidation prevented 0° fiber pullout. At 1,316 °C, a smooth glassy phase was observed in areas where degrading oxidation had occurred (this was not observed at 816 °C). In other regions, significant fiber pullout and embrittled regions with fiber breakage were observed at 1,316 °C.

6. Acoustic emission results provided early detection of cracking in the CMC in tensile tests and served as an alternative means to obtain PLS values in addition to conventional stress-strain curves in tensile strength tests.

7. Digital image correlation was able to identify high strain regions in the vicinity of the simulated cooling holes early in the tensile tests and tracked the damage as the load increased. DIC results also served as one more method to obtain PLS values.

References

1. Lewis, D., et al.: Application of Uncooled Ceramic Matrix Composite Power Turbine Blades for Performance Improvement of Advanced Turboshaft Engines. Annual Forum Proceedings—American Helicopter Society, vol. 64, no. 2, 2008, p. 1046.
2. Steibel, Jim: Ceramic Matrix Composites Taking Flight at GE Aviation. Am. Ceram. Soc. Bull., vol. 98, no. 3, 2019, pp. 30–33.
3. Kalluri, Sreeramesh, et al.: High Temperature Tensile Properties and Fatigue Behavior of a Melt-Infiltrated SiC/SiC Composite. Fatigue 2002, Proceedings of the Eighth International Fatigue Congress, Stockholm, Sweden, Volume 3/5, A.F. Blom, ed., Engineering Materials and Advisory Services, Ltd., EMAS, West Midlands, U.K., 2002, pp. 1965–1972.

4. Verrilli, Michael J.; Kalluri, Sreeramesh; and Kantzos, Peter T.: High-Cycle Fatigue Behavior of a Nicalon™/Si-N-C Composite. NASA/TM—1999-209383, 1999. https://ntrs.nasa.gov
5. Morscher, Gregory N.: Intermediate Temperature Stress Rupture of Woven SiC Fiber, BN Interphase, SiC Matrix Composites in Air. NASA/CR—2000-209927, 2000. https://ntrs.nasa.gov
6. Kalluri, Sreeramesh; Calomino, Anthony M.; and Brewer, David N.: Influence of R-Ratio on the Fatigue Behavior of a Woven SiC/SiC Composite. Mechanical Properties and Performance of Engineering Ceramics II: Ceramic Engineering and Science Proceedings, Rajan Tandon, Andrew Wereszczak, and Edgar Lara-Curzio, eds., John Wiley & Sons, Hoboken, NJ, 2007, pp. 245–256.
7. Morscher, Gregory N.: Stress-Dependent Matrix Cracking in 2D Woven SiC-Fiber Reinforced Melt-Infiltrated SiC Matrix Composites. Compos. Sci. Technol., vol. 64, no. 9, 2004, pp. 1311–1319.
8. Morscher, Gregory N.: Stress-Environmental Effects on Fiber-Reinforced SiC-Based Composites. Ceramic Matrix Composites: Materials, Modeling and Technology, Narottam P. Bansal and Jacques Lamon, eds., John Wiley & Sons, Hoboken, NJ, 2015, pp. 334–352.